GPS Amplitude Radio Holography: Application to Remote Sensing of the Atmospheric and Ionospheric Processes

A. G. Pavelyev and A.A. Pavelyev

Institute of Radio Engineering and Electronics Russian Academy of Sciences, Fryazino, Vvedenskogo sq. 1, 141191 Moscow region, Russia E-mail pvlv@ms.ire.rssi.ru

J. Wickert and T. Schmidt

(2) GeoForschungsZentrum Potsdam, Germany(GFZ-Potsdam), Telegrafenberg, 14473 Potsdam Germany E-mail: wickert@gfz-potsdam.de

Y.A. Liou

[3]Center for Space and Remote Sensing Research, National Central University, Chung-Li, 320, Taiwan.

E-mail: yueian@csrsr.ncu.edu.tw

K. Igarashi

National Institute of Information and Communications Technology, 4-2-1, Nukui-Kita Machi, Koganei-shi, Tokyo 184-8795 Japan E-mail:igarashi@nict.go.jp

Abstract. Since 1995, the global positioning system (GPS) has been exploited for remote sensing in the radio occultation (RO) scheme to obtain the vertical profiles of refractivity, temperature, pressure and water vapor in the neutral atmosphere and electron density in the ionosphere with global coverage. In the GPS RO scheme the GPS transmitter emits radio signal, which propagates through the ionosphere and the atmosphere, and then arrive at a receiver installed on the Low Earth Orbit (LEO) satellite. The receiver registers the phase and amplitude of the radio waves during the LEO orbital motion and produces two 1D radio holograms at two GPS frequencies f_1=1575.42 MHz and f_2=1227.6 MHz. The radio holographic approach (RFSA, CT, BP and other methods) can be used to reveal the vertical profiles of the physical parameters in the ionosphere and atmosphere along the trajectory of the motion of the tangent point, where the GPS signal trajectory has a minimal height above the Earth's surface. Applying the GPS RO remote sensing to the Earth's atmosphere study was demonstrated for the first time with the GPS/MET experiment. Since then several satellite missions have been launched with GPS occultation receivers including OERSTED, SUNSAT, CHAMP, SAC-C, and GRACE. Future RO remote sensing investigations that are planned now include ROCSAT3/COSMIC and Terra-SAR missions. This requires modernization of radio holographic methods in the RO remote sensing technology with the goal of heightening the accuracy and broadening the potential of the GPS RO remote sensing method. In this contribution a be new radio holographic amplitude method for GPS RO remote sensing is presented. This method allows one to measure the vertical gradients of the refractivity in the atmosphere and electron density in the lower ionosphere, monitoring the internal waves activity in the atmosphere, studying the ionospheric disturbances on a global scale. As follows new radio holographic method may be informative for investigations of the connections between processes in the atmosphere and mesosphere, analysis of the influence of the space weather phenomena on the lower ionosphere.
Keywords: Radio Holography, Radio Occultation, Atmosphere, Ionosphere, Refractivity, Electron Density

1 Introduction

Significant refinements and modernizations in the RO technique have been introduced in recent years. This has lead to an increase in the accuracy of the RO method and helped create the opportunity of devising new applications in geophysical researches. One potential application is in the investigation of gravity wave (GW) activities from temperature variations in the 5-40 km interval retrieved from the phase part of the GPS RO hologram [1-3]. As follows [1-3] atmospheric observations conducted by satellites with the GPS occultation method are powerful in examining the GW distribution around the world with an almost uniform quality. However, it is difficult to estimate key GW

parameters, such as the altitude distribution of their phase and amplitude, or intrinsic phase velocity by employing the phase of GPS signals.

The importance of the amplitude channel of the GPS radio holograms for the RO investigation of the atmosphere and ionosphere has been noted earlier [4-12]. In particular the different inherent sensitivities of the amplitude and phase of the RO signals to the wave structures in the atmosphere and ionosphere.has been established [10].

The goal of this paper consists in the application of the RO amplitude radio holographic method in investigating the atmosphere and ionosphere. In section 2 application of the amplitude method is considered for studying the vertical profiles of the electron density, and its gradient in the plasma layers in the lower ionosphere In section 3 the connection between the phase and amplitude variations in the RO signals is analyzed and the relationships for the retrieval of the refractivity and vertical temperature gradient are presented. It is shown that the amplitude of the RO signals is more sensitive than the phase to the wave structures in the atmosphere and ionosphere. In section 4 a possibility for measuring the internal GW parameters associated with GW horizontal wind perturbations is discussed using the GW polarization and dispersion relationships.

2. Local mechanisms of the RO amplitude variations

The main contribution to the amplitude of the RO signal under the case of a quiet ionosphere is introduced by a relatively small area along the ray GTL with the center situated at the tangent point T (Figure 1, left panel), where the ray trajectory is perpendicular to the local gradient of the refractivity. If precise orbital data are given, the height h of point T can be evaluated under an assumption of spherical symmetry of the ionosphere and atmosphere with the center at point O (Figure 1, left panel). For some RO experiments, strong amplitude scintillations have been observed at a height interval above the neutral atmosphere and below the E-layer of the ionosphere [6]. Moreover, sporadic amplitude scintillations have been indicated at GPS frequencies in trans-ionospheric satellite-earth links [13, 14]. Sporadic amplitude scintillations can be caused by plasma disturbances in the ionospheric E- and F-layers [13] In the absence of a global spherical symmetry, a new tangent point 1 can appear in the ionosphere, where sharp gradients of the electron density in an inclined plasma layer is perpendicular to the ray trajectory GTL (Figure 1, right panel). This point can appear on both sides of the ray GTL (GT or TL). In this case the height $h(T)$ of the observed RO amplitude variations depends on the inclination δ of the inclined plasma layer relative to the local horizontal direction (Figure 1, right panel). Consequently, the apparent height displacement Δh can arise from the estimated value of the inclined plasma layer's altitude (Figure 1, left panel). The layer's inclination δ and its horizontal displacement relative to point T d can be evaluated using Figure 1 (right panel)

$$\delta=(2\Delta h/r)^{1/2},\ d=(2\Delta hr)^{1/2},\ \Delta h=d^2/(2r), \qquad (1)$$

where r is the distance OT.

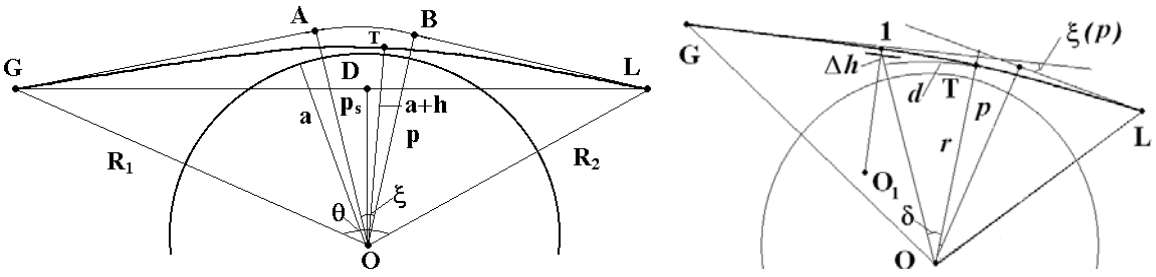

Figure 1. Left panel. Key physical parameters for estimation of the phase path excess of the RO signal in the case of global spherical symmetry of the refractivity distributions in the ionosphere and atmosphere. Right panel. Inclined plasma layer 1, where gradient of the electron density is perpendicular to the RO ray GTL, can be a possible cause of the amplitude scintillations measured at point L.

For the case of the quiet and spherical symmetric ionosphere, the technique of inversion of the amplitude data for finding the electron density and its gradient has been developed earlier [4,5], [8-12].

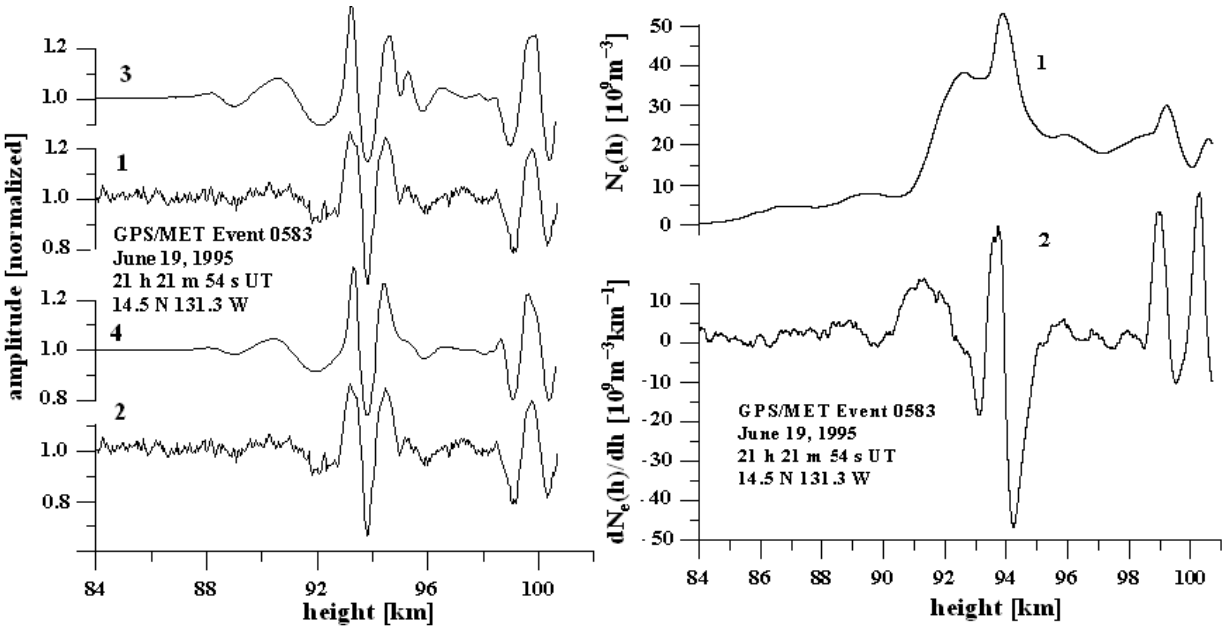

Figure 2. **Left panel. Amplitude variations in the RO signal. Curves 1 and 2 correspond to the experimental amplitude data at frequency F1 and F2, respectively; curves 3 and 4 are recalculated from the retrieved distribution of the vertical gradients of electron density. Right panel. The vertical profiles of the electron density and its gradient found from the amplitude variations.**

The experimental data and the retrieved electron density vertical profile are shown in Figure 2 for the GPS/MET event 0583 (June 19, 1995; 21 h 21 m UT; 14.5 N 131.3 W). Curves 1 and 2 in Figure 2, left panel, indicate the experimental data; smooth curves 3 and 4 in Figure 2, left panel, show the amplitude variations recalculated by ray tracing technology from the vertical profiles *dN(h)/dh, N(h)*. The results of the recalculation are quite close to the experimental data. Curves 1 and 2 in Figure 2, right panel, demonstrate the retrieved vertical gradient *dN(h)/dh* and electron density $N_e(h)$. The highest positive maximums of $dN_e(h)/dh$, which are seen at heights 93.5 and 101.5 km are equal to $25 \cdot 10^9$ and $33 \cdot 10^9$ [$m^{-3}km^{-1}$]. Two maximums (at levels 94.5 and 99 km) in the electron density are equal to $55 \cdot 10^9$ and $28 \cdot 10^9$ [$1/m^3$]. Results shown in Figure 2 illustrate the sensitivity of amplitude channels of the RO signal to variations of the vertical gradients of the electron density in the sporadic E-layers of the ionosphere.

Another application of the amplitude method is based on its high sensitivity to the plasma perturbations in the ionosphere. The amplitude variations of the RO signal shown below is described by the magnitude of the S_4 scintillation index [13]:

$$S_4 = 2[<(A(t) - <A>)^2> / <A>^2]^{1/2} \qquad (2)$$

where <> is the average relevant to the height interval $h(T)$ 40-80 km, and $A(t)$ is the amplitude of the RO signal. The amplitude data obtained during the CHAMP RO experiment described previously [15] was used for analysis.

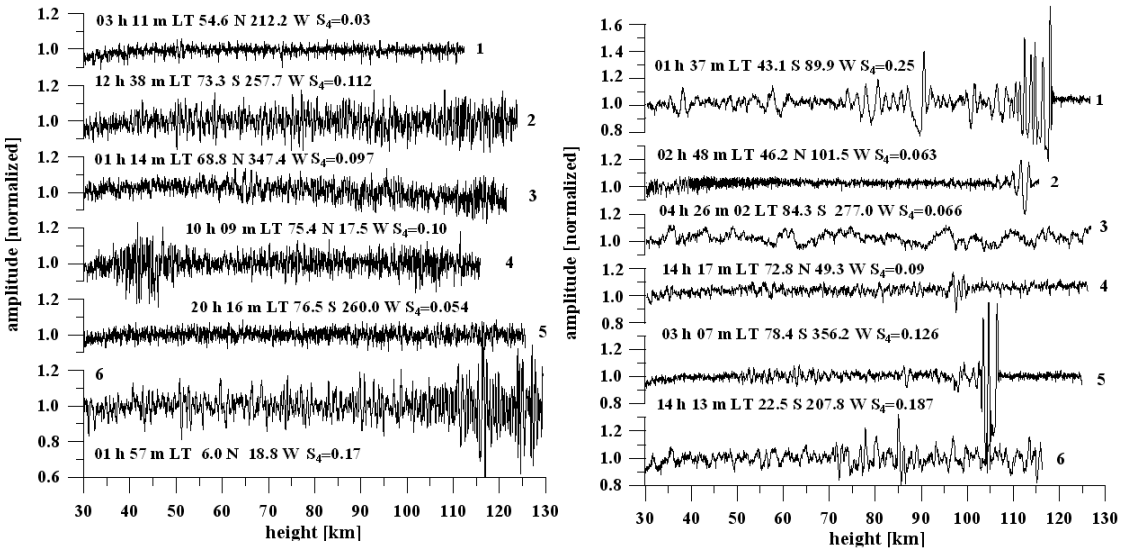

Figure 3. Left panel: C-type noisy amplitude scintillations of the RO signal. Right panel: S-type quasi-regular amplitude variation. Legends indicate the local time (LT) and the geographical coordinates of the RO experiments.

The CHAMP RO amplitude variations, which can be recognized as C- and S- types of the amplitude scintillations that have been observed previously [13] in the communication Inmarsat link at frequency 1.5 GHz, are shown in Figure 3.

The noisy C- type amplitude variations in the RO signals are shown in Figure 3, left panel. Curves 2, 3, 5, and 6 describe scintillations observed during the local daytime (curve 2), local evening and nighttime in the polar (north and south) region (curve 3 and 5) and in the equatorial region (curve 6) during RO events No. 0135 (curve 2); No. 0112 (curve 3); No. 0058 (curve 5); No. 0168 (curve 6), January 23, 2003. The S_4 index showed values of 0.112, 0.10, 0.054, 0.17, respectively. Event 0004 corresponded to the local morning (January 23) in the polar ionosphere, with S_4=0.10 (curve 4). Curve 1 is related to the quiet nighttime ionosphere, with S_4=0.03 (event No. 0030, January 23); the amplitude fluctuations in the height interval h(T) 30-110 km were caused mainly by random receiver noise. The geographical position and local time of the noisy RO events were in agreement to the same parameters of the noisy amplitude scintillations observed formerly in trans-ionospheric communications [14]. Noisy scintillations can be associated with small-scale plasma irregularities in the F- or E- layers of the ionosphere [13, 14].

Quasi-regular amplitude variations are shown in Figure 3, right panel. Curves 1, 2, 4 correspond to the CHAMP RO events 0078, 0096, 0171, January 23 (mid-latitude nighttime and polar daytime ionosphere); curves 3, 5 are related to events No. 0230, 0026, January 23; and curve 6 is associated to event No. 0040, January 23, 2003 (daytime equatorial ionosphere). The quasi-regular amplitude variations can be caused by inclined plasma layers in the E- or F-region of the ionosphere [15]. Apparent displacements in the height of a plasma layer Δh from its normal location can be applied to estimate the inclination δ and horizontal displacement d of the layer relative to point T (Figure 1, right panel) through employment of equation (1). However, the uncertainty in the sign of the horizontal displacement d and inclination δ exists because the ionospheric disturbance can be located at the same distance d from point T on the GT or LT part of the ray trajectory GTL (Figure 1, right panel). Note that application of the backward propagation (BP) method as shown in [6] provides a possible method in solving the task of localization of the ionospheric disturbances.

Quasi-regular amplitude variations can be used for restoring the electron density distribution and its vertical gradient under the assumption of a locally spherical and symmetric inclined ionospheric layer by a method described formerly [6]. For a demonstration, the CHAMP RO event (January 14, 2003, 0 h 56 m LT, 76.4 N, 172.7 W) with strong quasi-regular wave-like amplitude variations will be used.

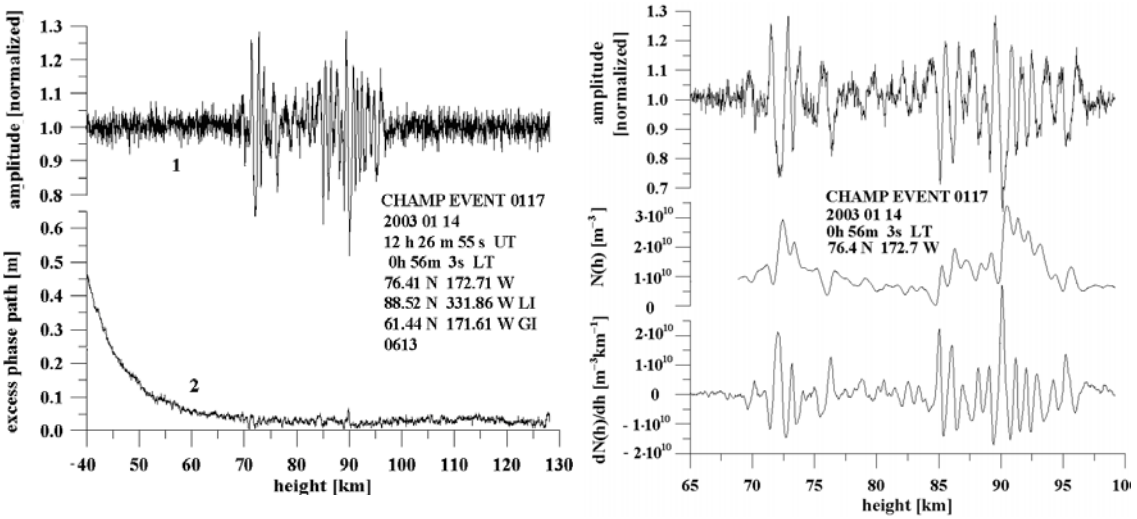

Figure 4. Left panel. Amplitude of the CHAMP RO signal (curve 1) and phase path excess at the combined frequency of F0 (curve 2) as functions of the height *h* at the ray tangent point T (Figure 1, right panel). S_4 index was equal to 0.12, which corresponded to the disturbed ionosphere. Right panel. The amplitude variations (top curve), the electron density distribution *N(h)* (middle curve) and the gradient of the electron density distribution *dN(h)/dh* (bottom curve) as functions of height *h* (Figure 1, right panel).

In Figure 4, left panel, the amplitude variations of the CHAMP RO signal are compared with the phase path excess at a combined frequency F0. The form of the amplitude variations indicate that the ionospheric disturbance consists of two connected patches, which are responsible for the maximum amplitude changes within the 72-76 km and 84-96 km intervals *h(T)*. In the 76-84 km interval, the amplitude variations are not so strong. Connection between the amplitude variations in two height intervals indicates that the ionospheric disturbance is a unified structure distributed in the horizontal and vertical directions. The phase variations at the frequency F0, as seen in Figure 4, left panel, are small. This reveals a fine quality of the ionospheric correction introduced in the phase data. The ionospheric correction has been conducted by the usual method of subtracting the ionospheric influence from the phase path excesses measured at GPS frequencies F1 and F2. The results of restoring the electron density distribution and its gradient are shown in Figure 4, right panel. The electron density variations are concentrated in the interval $0<N(h)<3.5\cdot10^{10}$ [electrons/m^{-3}]. These magnitudes of *N(h)* are somewhat below the usual values of *N(h)* for the sporadic E-layers. The height interval of the amplitude variations is nearly equal to the height interval of the variations in the electron density and its gradient. Following the estimation of the most probable location of both patches, the first patch is located on the line GT at a distance 300 km from the point T. It is concentrated in the 92-104 km interval with a negative inclination to the horizontal direction δ of about 3°. The second patch is located on the line GT in the 94-100 km interval at the distance 500 km relative to the tangent point T (Figure 1) with a negative inclination of about 5°.

3. Connection between the amplitude and phase variations

The variations in the phase and amplitude of the signals propagating along the ray GTL (Figure 1, right panel) can be described in the case of spherical symmetry [9] by relationships

$$\Phi(p)=L(p)+\kappa(p),\ \theta=\pi+\xi(p)-A(p),$$
$$L(p)=(R_2^2-p^2)^{1/2}+(R_1^2-p^2)^{1/2}-[(R_2^2-p_s^2)^{1/2}+(R_1^2-p_s^2)^{1/2}]+p\xi(p) \quad (3)$$

$$\xi(p)=A(p)-A(p_s);\ A(p)=\sin^{-1}(p/R_1)+\sin^{-1}(p/R_2),\ -d\kappa(p)/dp=\xi(p) \quad (4)$$

The relationships (3), (4) connect the phase path excess $\Phi(p)$ with the refraction angle $\xi(p)$, impact parameter p, and the main refractivity part of the phase path excess $\kappa(p)$. They are also valid for the rays in a multi-path situation. The refraction attenuation is described by formulas [16]

$$X(p)=pR_0^2[R_1R_2(R_2^2-p^2)^{1/2}(R_1^2-p^2)^{1/2}\sin\theta]^{-1}\ \left|\partial\theta/\partial p\right|^{-1} \quad (5)$$

where R_0 is the distance GDL (Figure 1, left panel). The refraction attenuation $X(p)$ depends mainly on the second derivative of the main refractivity part of the phase path excess $\kappa(p)$:

$$X(p)=[1/(R_2^2-p_s^2)^{1/2}+1/(R_1^2-p_s^2)^{1/2}]/\left|d^2\kappa/dp^2+1/(R_2^2-p^2)^{1/2}+1/(R_1^2-p^2)^{1/2}\right| \quad (6)$$

Consequently, the amplitude variations are more sensitive to the wave structures in the atmosphere and ionosphere than the phase path excess. The amplitude variations may be used for obtaining the height distribution of the vertical gradient of the refractivity. The solution of the inverse RO problem for the amplitude channel of the RO signal has been described previously [16]. For the case of circular orbits of the LEO and GPS satellites, this solution can be obtained using equations

$$dp/dt=X(t)p_s dp_s/dt \qquad p-p_0=\int X[t(p_s)]dp_s \quad (7)$$

Equations (7) can be used to find the vertical distribution of the vertical refractivity gradient $dN(h)/dh$ [11,12]:

$$dN(h)/dh=-n^2(h)J(p)/\{p[1+J(p)]\};\quad J(p)=1/\pi\int d^2\xi(x)/dx^2(x^2-p^2)^{1/2}dx$$
$$p=n(h)(a+h),\ n(h)=1+N(h)*10^{-6},\ d\xi(p)/dp=B(p)(X-1)/X \quad (8)$$

Integration in (8) is performed from p to infinity.

The amplitude information may be used to retrieve the vertical gradient of the temperature profile [11,12]:

$$[dT^*(h)/dh]/T^*(h)=-[N(h)]^{-1}dN(h)/dh-T_x/T_a(h)$$
$$T^*(h)=T(h)/\{1+4810e(h)/[P(h)T(h)]\},T_x\approx 34.16K/km, \quad (9)$$
$$T_a(h)=T(h)[1+0.378e(h)/P(h)]$$

where $T(h)$ is the temperature of the atmosphere [K], $T^*(h)$ is the "wet" temperature of the atmosphere depending on the water vapor pressure $e(h)$ and atmospheric pressure $P(h)$ [hPa], respectively. Equation (9) connects the vertical gradient of the logarithm of the refractivity with the vertical gradient of the logarithm of the "wet" temperature $T^*(h)$. At the height above 10 km, equations (9) may be used to find the vertical gradient of the temperature profile if the refractivity gradient is known. Integration of the first equation (9) produces the vertical profile $T(h)$ if an initial condition is known at some height h_1 [18]

$$T^*(h)=T^*(h_1)N(h_1)/N(h)+T_x/N(h)\int N(h)dh/\{(1+0.38e/p)[1+4810e/(pT)]\}dh \quad (10)$$

where the integration is performed from h to h_1.

Equations (5)-(9) are useful for estimating the vertical gradients of the refractivity and temperature, and the parameters of the wave structures in the atmosphere and ionosphere.

4. Amplitude variations and wave structures in the atmosphere

Below, we will consider the perturbations in the vertical temperature gradient to establish the parameters of the wave structures in the atmosphere. The amplitudes of the RO signal are shown in Figure 5, left panel, for the CHAMP RO event 0005 (curve A) and GPS/MET RO event 0316 (curves A1, A2). Simulation results of the amplitude dependence on height are shown in Figure 5, left panel, by the curves M0 and M. For the calculation of the M0, the refractivity model $N(h)=N_o exp(-h/H)$ with $N_o=340$ *(N-units)* and $H=6.4$ *km* is used, along with the analytical connections between the refraction angle $\xi(p)$, the refraction attenuation, and the refractivity gradient described above. The same method was applied in obtaining the curves M in Figure 5, left panel, but the refractivity model was a sum of the damped complex exponentials $N(h)=Re[N_j exp(-\alpha_j h)]$ with real and complex N_j and α_j. The parameters N_j and α_j have been determined in a way to provide the amplitude variations, which better coincide with the experimental data. To obtain the vertical profiles of the temperature and its gradient, we use the expressions (6)-(9). The vertical gradients of the temperature retrieved from the amplitude data are indicated for the CHAMP (the bottom curves A and M) and GPS/MET RO (the upper curves A1, A2 and M) events 0005 and 0316 in Figure 5, right panel. Note that in the CHAMP RO experiments, only the amplitude variations at the first GPS frequency F1 have been measured. The curves M in Figure 5, right panel, indicate the simulation results relating to the CHAMP (the second curve from bottom in Figure 5, right panel) and GPS/MET (the second upper curve in Figure 5, right panel) RO events; the curves A1, A2, and A describe the vertical temperature gradient variations restored from the initial amplitude changes shown in Figure 5, left panel. It is evident from the right panel of Figure 5, that the wave activity in the atmosphere is a function of height. The maximum wave activity is observed in the tropopause region in the 12-17 km interval, and the secondary maxima of the wave activity can be seen within the 22-27 km interval of the stratosphere. Quasi-regular wave structures with vertical wavelength $\lambda_v \sim 0.8–2$ *km* are clearly seen in both the experimental and model data. The observed waves in the altitude distributions of the

amplitude and vertical temperature gradient can correspond to the GW activity. If the observed wave structures are caused by the GW activity, the vertical temperature gradients can be related with the horizontal wind perturbations. The magnitude of the horizontal wind perturbations can be estimated from the polarization relationships, which are valid for medium-frequency cases, when the intrinsic frequency of the GW is greater than the inertial frequency *f*, but is well below the buoyancy frequency ω_b. The GW dispersion relation has the form [19,20]:

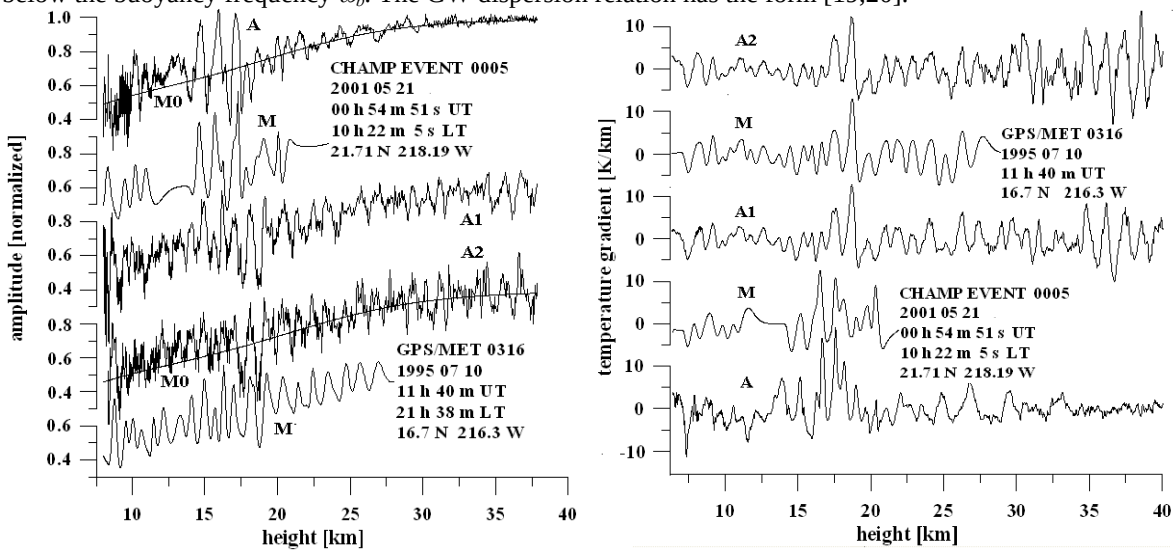

Figure 5. Left panel: wave trains in the GPS/MET and CHAMP RO amplitude data. The legend indicates the time of the RO experiments and the geographical co-ordinates of the RO regions. Right panel: temperature gradient variations for the GPS/MET and CHAMP RO events.

$$\lambda_v = 2\pi / |c - U\cos\varphi| / \omega_b \qquad (11)$$

where λ_v is the vertical wavelength of the GW, U is the background wind speed, c denotes the ground-based GW horizontal phase speed, and φ is the azimuth angle between the background wind and the GW propagation vectors. Equation (11) connects the vertical wavelength λ_v with the intrinsic phase speed of the GW $v_i = |c - U\cos\varphi|$, which can be measured by an observer moving with the background wind velocity [20]. A GW polarization relation was published previously [21], which links the complex amplitude of the temperature variation, *t(h)* with the horizontal wind perturbations *v(h)*, and also enjoys a correspondence with the GW influence

$$v = Re[ig/(T_b\omega_b)t(h)] \qquad (12)$$

where $\omega_b^2 = g/T_b\Gamma$, $\Gamma = \partial T_b/\partial h + 9.8^o/km$, g is the gravity acceleration, and T_b is the background temperature. One can obtain a connection between the vertical gradients *dv(h)/dh* and *dt(h)/dh* from (12)

$$dv(h)/dh = dRe[ig/(T_b\omega_b)t(h)]/dh \approx Re[ig/(T_b\omega_b)dt(h)/dh \qquad (13)$$

Equation (13) is valid under assumption that $T_b(h)$ and $\omega_b(h)$ are slowly changing at the vertical scales $\sim\lambda_h$. The functions T_b and ω_b in equation (13) are known from the atmospheric model, which is used for the calculation of the refraction attenuation and refractivity in the RO region. To find the function *dv(h)/dh* from the second equation (13), one can implement the radio holographic analysis through the Hilbert transform [22]. Application of the Hilbert transform gives an analytic presentation of the real signal *dt(h)/dh*:

$$dt(h)/dh = Re\{a_t(h)\exp[i\Phi_t(h)]\} \qquad (14)$$

where $a_t(h)$ and $\Phi_t(h)$ (real functions) are the amplitude and phase of the temperature vertical gradient. The function *dv(h)/dh* can further be restored from (14) by employing the Hilbert transform to both the experimental and model data. The results of the vertical gradient restoration of the horizontal wind perturbations are indicated in Figure 6 (left panel). The upper curves (A1, A2, M) in Figure 6 (left panel) are in accordance to the vertical gradient of the horizontal wind perturbations restored from the GPS/MET RO event 0316, while the bottom two curves (M, A) are related to the CHAMP RO event 0005. The quasi-regular modulation of *dv/dh* from the wave structures in the atmosphere can be clearly witnessed from both the experimental and model data. It is important that the vertical period of this modulation is

practically the same as seen in the amplitude variations in Figure 6, left panel. After application of the Hilbert transform, one can obtain from (13) and (14) the amplitude $a(h)$ and phase $\Phi(h)$ that is associated with the vertical gradient of the horizontal wind perturbations $dv(h)/dh = a(h)\cos\Phi(h)$. The two variables $a(h)$ and $\Phi(h)$ indicate the amplitude and phase of the analytic signal relevant to $dv(h)/dh$. The functions $a(h)$ and $\Phi(h)$ together present a 1-D radio image of GW or GW "portrait". The height dependence of the GW phases $\Phi(h)$ and amplitudes $a(h)$ are shown in Figure 6 (right panel) by curves 1, 2 and 3, 4, respectively, for the GPS/MET and CHAMP RO events 0316 and 0005.

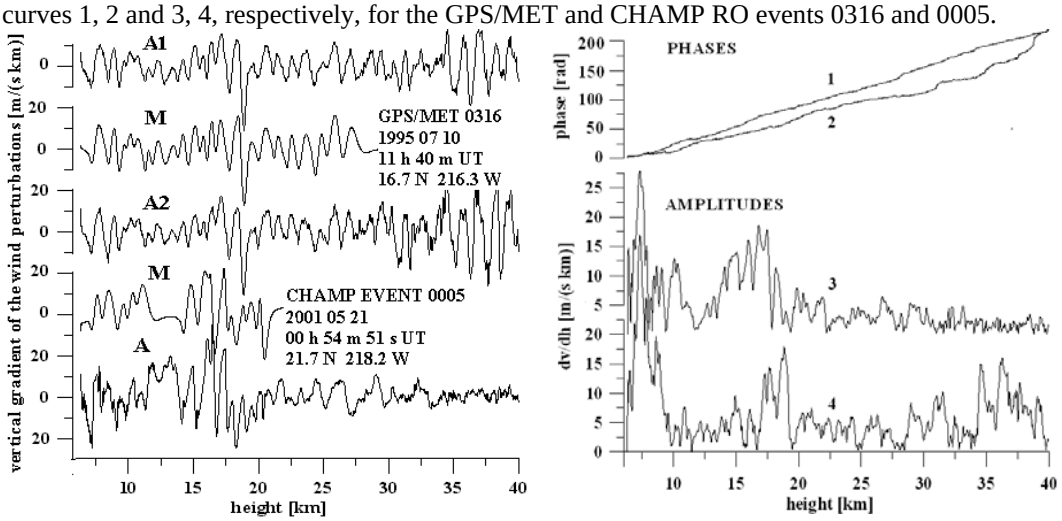

Figure 6. Left panel: vertical gradient of the horizontal wind perturbations retrieved from the variations of the vertical temperature gradient for the GPS/MET (three upper curves) and CHAMP (two bottom curves) RO events. Right panel: comparison of the GW portraits found from the wave trains in the amplitude indicates an increase of the spatial frequency of the GW with height. The phase in the GPS/MET event (curve 1) changes monotonically, in average, as a function of height h; thus corresponding to a quasi-monochromatic GW. The amplitude, relevant to the GPS/MET event (curve 3), demonstrates essential changes in the interval 0.5...16 m/(s km) above 10 km. For this event, one can see altitudes with high (17-19 km, 29-31 km, 35-38 km) and low (32-34 km) GW activities. For the CHAMP RO event (curve 4), the amplitude changes are concentrated mainly below 20 km.

The foregoing proves the importance of the RO radio holographic amplitude method in investigating GW with global coverage.

5. Conclusions

Amplitude variations of RO signals are more sensitive to the sharp gradients of the refractivity in the ionosphere and atmosphere than the phase path excess. This sensitivity is attributable to dependence of the refraction attenuation on the second derivative of the main refractivity part of the phase path excess on the impact parameter. This inherent property of the amplitude variation opens the opportunity for new applications of the RO method in the remote sensing of the atmosphere and ionosphere from space in the trans-ionospheric satellite-satellite and satellite-to-Earth links.

The amplitude variations of the RO signal significantly depend on the vertical structure of the upper troposphere and stratosphere. The perturbations in the vertical gradient of the refractivity can be found directly from the amplitude variations of GPS signals. The temperature perturbations and their vertical gradients in the atmosphere can also be retrieved.

Amplitude variations are, in essence, the 1-D radio holographic image of the internal waves in the atmosphere. The RO amplitude variations can be applied to find the phase and amplitude of the GW as a function of height. By subsequently using the GW polarization relationships, one can find the horizontal wind perturbations and its vertical gradient as a function of the altitude. Preliminary comparison of the horizontal wind perturbations obtained from the amplitude data analysis with the radiosondes data reveals a good correspondence. Radio holographic analysis of the CHAMP RO amplitude data has shown the possibility of revealing locations of GW breaking regions in the stratosphere, which in addition to the data obtained from the RO phase data, introduces another complementary source of information on the stratospheric physical conditions.

The amplitude of the GPS signal is a radio holographic indicator of the ionospheric disturbances in the trans-ionospheric links. The amplitude variations of GPS signals are corresponding to two types of the amplitude variations (noisy and quasi-regular) previously observed in the satellite-Earth trans-ionospheric links. Quasi-regular amplitude variations can be inversed to obtain the electron density distribution and its gradient in the ionospheric layers.

It follows that the amplitude part of the GPS RO radio hologram is an important source of the information on the wave phenomena in the atmosphere and ionosphere. The amplitude variations can be used for experimental studying the connections between the processes in the atmosphere, mesosphere and ionosphere.

Acknowledgements. The authors gratefully acknowledge GFZ-Potsdam for delivering the CHAMP and GPS/MET RO data for analysis. The work is partly supported by the Russian Fund of Basic Research, grant No. 03-02 17814, Taiwan grant 92-NSPO (B)-RS3-FA07-03 and Russian programs OFN-16 and OFN-17.

References

[1] Steiner, A. K., and G. Kirchengast 2000 GW spectra from GPS/MET occultation observations. *J. Atmos. Ocean. Tech.,* **17**. 495-503.

[2] Tsuda T., M. Nishida, C. Rocken, and R.H. Ware 2000 A global morphology of GW activity in the stratosphere revealed by the GPS occultation data (GPS/MET). J. Geophys. Res. **105.** 7257-7273.

[3] Tsuda T., and K. Hocke 2002 Vertical wave number spectrum of temperature fluctuations in the stratosphere using GPS occultation data. *J. Meteorol. Soc. Japan,* **80**. 4B. 1-13.

[4] Igarashi, K., A. Pavelyev, K. Hocke, D. Pavelyev, and J. Wickert 2001 Observation of wave structures in the upper atmosphere by means of radio holographic analysis of the RO data. *Adv. Space Res*. **27**. 6-7. 1321-1327.

[5] Igarashi, K., A. Pavelyev, K. Hocke, D. Pavelyev, I.A. Kucherjavenkov, S. Matugov, A. Zakharov, and O. Yakovlev 2000 Radio holographic principle for observing natural processes in the atmosphere and retrieving meteorological parameters from RO data. *Earth Planets Space*. **52**. 968-875.

[6] Sokolovskiy, S.V., W. Schreiner, C. Rocken, and D. Hunt 2002 Detection of high-altitude ionospheric irregularities with GPS/MET. *Geophys.Res. Lett.,* **29**. 3. 621-625.

[7] Sokolovskiy, S.V. 2000 Inversion of RO amplitude data. *Radio Sci.*, **35**. 1. 97-105.

[8] Pavelyev A., K. Igarashi, C. Reigber, K. Hocke, J. Wickert, G. Beyerle, S. Matyugov, A. Kucherjavenkov, D. Pavelyev, O. Yakovlev 2002 First application of radioholographic method to wave observations in the upper atmosphere. *Radio Sci.,* **37**(3), 15-1 –15-11.

[9] Pavelyev A.G., T. Tsuda, K. Igarashi, Y.A. Liou, and K. Hocke 2003. Wave structures in the electron density profile in the ionospheric D and E-layers observed by radio holography analysis of the GPS/MET radio occultation data, *J. Atmos. Solar-Terr. Phys*. **65**(1), 59-70.

[10] Pavelyev A.G., Y. A. Liou, J. Wickert 2004 Diffractive vector and scalar integrals for bistatic radio holographic remote sensing *Radio Sci.,***39**(4), RS4011, 1-16, doi:10.1029/2003RS002935.

[11] Liou, Y.-A., A.G. Pavelyev, C.-Y. Huang, K. Igarashi, and K. Hocke 2002 Simultaneous observation of the vertical gradients of refractivity in the atmosphere and electron density in the lower ionosphere by RO amplitude method. *Geophys.Res. Lett.* **29**. 19. 43-1 – 43-4.

[12] Liou, Y.-A., A.G. Pavelyev, C.-Y. Huang, K. Igarashi, K. Hocke, and S. K. Yan 2003 Analytic method for observation of the GW using RO data. *Geophys.Res. Lett.* **30**. 20. ASC 1-1 – 1-5.

[13] Karasawa, Y., K. Yasukawa, M. Yamada 1985 Ionospheric scintillation measurement at 1.5 GHz in mid-latitude region, *Radio Sci.*, 20(3), 643-651.

[14] Yeh, K.C., and C.H. Liu 1982 Radio wave scintillations in the ionosphere. *Proc. IEEE, 70(4)*, 324-360.

[15] Wickert J., A. G. Pavelyev, Y.A. Liou, T.Schmidt, Ch. Reigber, K. Igarashi, A.A. Pavelyev, and S.S. Matyugov 2004 Amplitude scintillations in GPS signals as a possible indicator of ionospheric structures *Geophys.Res. Lett.*, 31(24), L24801 doi:10.1029/2004GL020607, 1-4.

[16] Pavelyev A.G., and A.I. Kucherjavenkov 1978 Refraction attenuation in the planetary atmosphes. *Radio Eng. and Electron. Phys.* **23.** 7. 13-19.

[17] Kalashnikov, I., S. Matugov, Pavelyev A., and O. Yakovlev 1986 Analysis of the features of RO method for the Earth's atmosphere study. In the book *Electromagnetic waves in the atmosphere and space.* 208-218. "Nauka" Ed. Moscow (in Russian).

[18] Hocke, K. 1997 Inversion of GPS meteorology data. *Annales Geophysicae* 15, 443-450.

[19] Eckermann S.D., I. Hirota, and W.A. Hocking 1995 GW and equatorial wave morphology of the stratosphere derived from long-term rocket soundings. *Q.J.R. Meteorol. Soc*. 121. 149-186.

[20] Fritts D.C., and M.J. Alexander 2003 GW dynamics and effects in the middle atmosphere. *Rev. Geophys.*, 41, pp 3-1-3-64.

[21] Lindzen R.S. 1981 Turbulence and stress owing to GW and tidal breakdown. *J. Geophys. Res.* **86**(C-9), 707-714.

[22] Rabiner L. and B. Gold 1978 Theory and Application of Digital Signal Processing. Prentis Hall.